Article:
Wang, J, Zhang, Y, Zhang, C et al. (2023) Validating HONO as an Intermediate Tracer of the External Cycling of Reactive Nitrogen in the Background Atmosphere. Environmental Science & Technology, 57 (13). pp. 5474-5484. ISSN: 0013-936X

https://doi.org/10.1021/acs.est.2c06731

Validating HONO as an intermediate tracer of the external cycling of reactive nitrogen in the background atmosphere

Journal:	*Environmental Science & Technology*
Manuscript ID	es-2022-067318
Manuscript Type:	Article
Date Submitted by the Author:	14-Sep-2022
Complete List of Authors:	Wang, Jianshu; Peking University, State Key Joint Laboratory of Environmental Simulation and Pollution Control, College of Environmental Sciences and Engineering Zhang, Yingjie; Peking University, State Key Joint Laboratory for Environmental Simulation and Pollution Control, College of Environmental Sciences and Engineering; Beijing Forestry University, School of Ecology and Nature Conservation Zhang, Chong; Peking University, State Joint Key Laboratory of Environmental Simulation and Pollution Control, College of Environmental Science and Engineering Wang, Yaru; Peking University, State Key Joint Laboratory for Environmental Simulation and Pollution Control, College of Environmental Sciences and Engineering Zhou, Jiacheng; Chinese Academy of Sciences Hefei Institutes of Physical Science Anhui Institute of Optics and Fine Mechanics, Laboratory of Atmospheric Physico-Chemistry Whalley, Lisa; University of Leeds, School of Chemistry Slater , Eloise; University of Leeds, School of Chemistry Dyson, Joanna; University of Leeds, School of Chemistry; British Antarctic Survey Xu, Wanyun; Chinsese Academy of Meterological Sciences, Institute of Atmospheric Composition cheng, peng; Jinan University, Institute of Mass Spectrometry and Atmospheric Environment Han, Baobin; Jinan University, Institute of Mass Spectrometry and Atmospheric Environment Wang, Lifan; Peking University, State Key Joint Laboratory of Environmental Simulation and Pollution Control, College of Environmental Sciences and Engineering Yu, Xuena; Peking University, State Key Joint Laboratory of Environmental Simulation and Pollution Control, College of Environmental Sciences and Engineering Wang, Youfeng; Peking University, State Key Joint Laboratory of Environmental Simulation and Pollution Control, College of Environmental Sciences and Engineering Woodward-Massey, Robert; Peking University, State Key Joint Laboratory of Environmental Simulation and Pollution Control, College of Environmental Sciences and Engineering Lin, Weili; Minzu University of China, Key Laboratory of Ecology and Environment in Minority Areas Zhao, Weixiong; Anhui Institute of Optics and Fine Mechanics, Zeng, Limin; Peking University, State Key Joint Laboratory of

	Environmental Simulation and Pollution Control, College of Environmental Sciences and Engineering Ma, Zhiqiang; China Meteorological Administration Beijing Institute of Urban Meteorology Heard, Dwayne; University of Leeds Ye, Chunxiang; Peking University, State Key Joint Laboratory of Environmental Simulation and Pollution Control, College of Environmental Sciences and Engineering

Validating HONO as an intermediate tracer of the external cycling of reactive nitrogen in the background atmosphere

*Jianshu Wang, Yingjie Zhang, Chong Zhang, Yaru Wang, Jiacheng Zhou, Lisa K. Whalley, Eloise J. Slater, Joanna E. Dyson, Wanyun Xu, Peng Cheng, Baobin Han, Lifan Wang, Xuena Yu, Youfeng Wang, Robert Woodward-Massey, Weili Lin, Weixiong Zhao, Limin Zeng, Zhiqiang Ma, Dwayne E. Heard, and Chunxiang Ye **

ABSTRACT

In the urban atmosphere, nitrogen oxides (NO_x=NO+NO_2)-related reactions dominate the formation of nitrous acid (HONO). Here, we validated an external cycling route of HONO and NO_x, i.e., formation of HONO resulting from precursors other than NO_x, in the background atmosphere. A chemical budget closure experiment of HONO and NO_x was conducted at a background site on the Tibetan Plateau and provided direct evidence of the external cycling. An external daytime HONO source of 100 pptv h^{-1} was determined. Both soil emissions and photolysis of nitrate on ambient surfaces constituted likely candidate mechanisms characterizing this external source. The external source dominated the chemical production of NO_x with HONO as an

intermediate tracer. The OH production was doubled as a result of the external cycling. A high $HONO/NO_x$ ratio (0.31±0.06) during the daytime was deduced as a sufficient condition for the external cycling. Literature review suggested the prevalence of high $HONO/NO_x$ ratios in various background environments, e.g., polar regions, pristine mountains and forests. Our analysis validates the prevalence of the external cycling route in general background atmosphere and highlight the promotional role of external cycling regarding the atmospheric oxidative capacity.

KEYWORD

nitrous acid (HONO), reactive nitrogen, budget analysis, photochemistry, atmospheric oxidative capacity, the Tibetan Plateau

SYNOPSIS

Our data suggests a revision of reactive nitrogen chemistry and the oxidative capacity of the atmosphere.

TOC

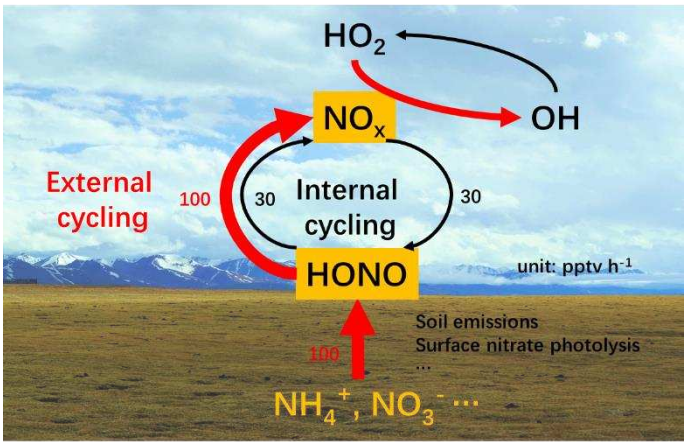
HO2
NOx
OH
External cycling
100
30
Internal cycling
30
HONO
unit: pptv h-1
Soil emissions
Surface nitrate photolysis
...
100
NH4+, NO3- ···

Introduction

In the urban atmosphere, nitrous acid (HONO) is distributed at concentrations ranging from hundreds of pptv to several ppbv. Solar radiation extending to up to 400 nm photolyzes HONO to produce OH radicals and NO (R1). The HONO photolysis frequency can reach 1.6×10^{-3} s^{-1} (ca. HONO lifetime of 10.4 min) at solar noon (solar zenith angle = 0°). HONO is therefore a primary precursor of OH radicals and greatly impacts the atmospheric oxidative capacity in such environments[1–3].

$$HONO + h\nu \rightarrow OH + NO \quad (R1)$$

$$NO + OH + M \rightarrow HONO + M \quad (R2)$$

$$NO_2 + surface \xrightarrow{(h\nu)} HONO \quad (R3)$$

The primary HONO emissions from vehicles can be characterized by a $HONO/NO_x$ emission ratio of 0.008[4]. However, a typical daytime $HONO/NO_x$ ratio of 0.02 is accompanied by a high abundance of HONO in the urban atmosphere[5]. This underlines the dominating role of chemical production in the HONO budget and in raising the $HONO/NO_x$ ratio. NO_x-related reactions, i.e., homogeneous reactions of NO with OH radicals (R2) and the heterogeneous conversion of NO_2 on environmental surfaces (R3), are generally accepted HONO formation mechanisms in such environments[6,7]. Under the photo-stationary state assumption (PSS) of HONO, equilibrium is established between HONO photolysis (R1) and HONO production from NO_x-related reactions. Assuming a pseudo-first-order R2 reaction rate of 1.16×10^{-5} s^{-1} (at an OH radical concentration of 10^6 molecule/cm^3 and temperature of 273 K)[8] and a HONO photolysis frequency of 1.6×10^{-3} s^{-1} under solar zenith angle $\Theta = 0°$, the PSS HONO/NO ratio is calculated as 0.007. The pseudo-first-order reaction rate of R3 on the ground surface is observed within the range of 0.004-0.033 h^{-1} without light enhancement[9], resulting in a corresponding PSS $HONO/NO_2$ ratio range of 0.0007-0.006. The slow turnover rate of NO_x to HONO compared to that of HONO to NO_x characterizes

a PSS HONO/NO_x ratio that is not significantly higher than the primary emission ratio. Solar radiation enhances heterogeneous NO_2 conversion (R3, hv) by one order of magnitude[10] and promotes the PSS HONO/NO_x ratio by the same magnitude, which could account for the typical PSS HONO/NO_x ratio of 0.02 in the urban atmosphere. The R1-R3 reactions are referred to as the internal cycling routes of HONO and NO_x, and there is no net production of HONO or NO_x in the internal cycling under the photo-stationary state of HONO.

Compared to the urban atmosphere where internal cycling chemistry dominates, substantially higher PSS HONO/NO_x ratios have been observed with lower HONO and NO_x levels in polar areas[11–15]. External sources, i.e., formation mechanisms with HONO precursors other than NO_x, are proposed in such environments. Upward HONO and NO_x fluxes from ice and snow surfaces point to enhanced photolysis of nitrate deposited on ice and snow surfaces as one external source of HONO and NO_x[11,16]. The concept of a quasi-liquid layer on snow and ice surfaces has been further constructed to account for the surface-catalyzed photolysis of nitrate, which occurs nearly one order of magnitude faster than the photolysis of gaseous nitric acid[17]. Such an external source dominates the HONO source budget and naturally also serves as a source of NO_x via external HONO photolysis in polar areas where primary NO_x emissions are negligible. OH production is greatly promoted as a result of the presence of external sources of HONO and NO_x[15,16]. Compared to internal cycling, which is initialized and accelerated by primary anthropogenic NO_x emissions in the urban atmosphere, external cycling in polar regions is driven by natural conditions, i.e., ubiquitous ambient surface and solar radiation conditions, implying its universal significance in the atmosphere.

Herein, we raise scientific questions regarding whether such external cycling of reactive nitrogen is prevalent in general background atmosphere and how external cycling perturbs the

oxidative capacity of these environments. The Tibetan Plateau is referred to as the third pole of the world, representing the global background of the atmosphere. With an average altitude of over 4000 m, the Tibetan Plateau features high solar radiation and notably intense photochemistry. The natural conditions of the Tibetan Plateau facilitate external cycling of reactive nitrogen analogous to the process prevailing in polar regions. During the in-depth study of atmospheric chemistry performed over the Tibetan Plateau in 2019, referred to as the @Tibet 2019 field campaign, we collected a comprehensive dataset related to HONO and NO_x budgets, the first dataset of its kind available for a background site on the Tibetan Plateau. This dataset allows direct validation of the external cycling of reactive nitrogen with HONO as an intermediate tracer and its role in promoting the atmospheric oxidative capacity via a near-explicit chemical model. A HONO/NO_x ratio that is unreasonably higher than the internal cycling mechanism permits is summarized as a sufficient condition for external cycling. A literature review suggests the prevalence of such unreasonably high ratios and, therefore, of an external cycling route present in general background atmosphere.

Materials and Methods

Measurements. Under the umbrella of the second Tibetan Plateau Scientific Expedition and Research Program (STEP), the field campaigns “In-depth Study of the Atmospheric Chemistry over the Tibetan Plateau: Measurement, Processing and the Impacts on Climate and Air Quality” (referred to herein as @Tibet 2019) was carried out at the Nam Co Multisphere Observation and Research Station (30°46.44′N, 90°59.31′E, 4730 m a.s.l.) from 28 April to 10 July 2019. The site was covered by alpine steppe with sparse vegetation during the measurement period. With very limited anthropogenic emissions, including visiting vehicles and pasture activities around the station, the Nam Co site is considered a background site.

Container measurements included HONO, NO_2, OH radicals, peroxyacetyl nitrate (PAN), O_3, CO, volatile organic compounds (VOCs), oxygenated VOCs (OVOCs), photolysis frequency of HONO, NO_2, and O_3, meteorological parameters, and the HONO flux, satisfying the calculation of HONO and NO_x budgets. The measurement methods are briefly described below.

HONO was measured by a commercial LOng-Path Absorption Photometer (LOPAP-03, QUMA), characterizing a wet chemical sampling and photometric detection technique[18]. In this study, 0.05 M sulfanilamide (SA) in a 0.1 M HCl was used as the scrubbing solution for gaseous HONO and 0.5 mM N-(1-naphthyl) ethylenediamine dihydrochloride (NEDA) was used for derivatization. The HONO was sampled with a two-channel coil, and HONO concentration was calculated by subtracting the signal in the second channel from that in the first channel to minimize possible interference (e.g., from PAN or NO_2). Zero air measurements were measured every 2 h for 30 min to correct for the instrument baseline fluctuations. A liquid nitrite standard calibration was performed to renew the calibration curve every week. The detection limit of the LOPAP was 5 pptv ($\pm 3\ \sigma$) with a time resolution of 3 min. The uncertainty of the LOPAP measurements mainly came from variations in the liquid flow rate and changes in the purities of the reagents, with a final uncertainty of 25%[18]. In this campaign, gaseous HONO was sampled at a tower at heights of 1.8 m and 6.8 m with a time cycle of 15 min to satisfy the measurement of HONO flux.

HONO flux was obtained by integrating the eddy covariance method (EC) and the Atmospheric gradients method (AG). The turbulent diffusion coefficient (k) was derived from the H_2O flux measured with eddy covariance method and water vapor density gradient, thus providing the real-time k required in the HONO flux calculation. The continuous HONO mixing ratio was obtained via interpolation, and the HONO gradients between 1.8 m and 6.8 m were then calculated. The HONO flux was then calculated using the k value and HONO gradients.

NO_2 was measured by an incoherent broadband cavity-enhanced absorption spectrometer (BBCES)[19]. Briefly, incoherent light centered at 460 nm was emitted from a blue light-emitting diode (LED), coupled in a light fiber and collimated with a SMA collimator before entering a 1-m Teflon optical cavity with highly reflective mirrors (R>99.9%) on both ends. The light was reflected multiple times before being transmitted and detected by a spectrometer (Ocean Optics, QE65000). The NO_2 mixing ratio was obtained by applying a least-squares fitting to the optical extinction coefficient and reference absorption cross-section of NO_2 over the wavelength range of 446-466 nm. The wavelength-dependent reflectivity of mirrors was determined weekly to calibrate the optical extinction coefficient of NO_2 in this system. The detection limit of NO_2 was 25 pptv (1σ) with a time resolution of 36 s. The uncertainty of the system was estimated to be 4%.

OH radicals were measured with a fluorescence assay by gas expansion (FAGE) instrument as described elsewhere[20]. Nonmethane VOCs and OVOCs were measured by online gas chromatography-mass spectrometry (GC-MS/FID, TH-PKU 300B, Wuhan Tianhong Instrument Co. Ltd., China) with a measurement method described elsewhere[20]. PAN was detected by a commercial analyzer (Metcon, Germany) consisting of an automated gas chromatograph equipped with an electron capture detector and a calibration unit. O_3 was measured by a commercial Ultra-Visible photometer (49C, Thermo Scientific™, MA, USA). CO and CH_4 were measured by a commercial analyzer based on wavelength-scanned cavity ring-down spectroscopy (PICARRO G2401). Photolysis frequencies were measured with a spectroradiometer (Metcon CCD-Spectrograph). Meteorological parameters, including temperature, pressure, precipitation, and water vapor pressure, were measured by the DZZ4 Automatic Weather Station.

Data observed from 2 – 20 May were averaged to the hourly resolution and used for analysis and model constraints in this study, as these parameters related to the HONO and NO_x budgets,

and OH radical production were most complete during this period. The list and time series of these parameters are shown in Table. S1 & Figure S1.

Budget calculation. Calculations of HONO and NO_x budgets, and OH radicals production were conducted by relying on field-measured parameters, published chemical kinetic data and model-calculated concentrations. The budget of each species was calculated with Eqs. 1-5 below.

$$P_{HONO} = k_{\mathrm{NOOH}}[\mathrm{NO}]_{mod}[\mathrm{OH}] + k_{het}[\mathrm{NO_2}] + \frac{\text{HONO flux}}{\mathrm{MLH}} + j_{pNO3}[\mathrm{pNO_3^-}] + External_{unaccounted} \quad \text{Eq.1}$$

$$D_{HONO} = j_{HONO}[\mathrm{HONO}] - \frac{v_{HONO}}{BLH}[\mathrm{HONO}] \quad \text{Eq.2}$$

$$P_{NO_x} = j_{HONO}[\mathrm{HONO}] + \mathrm{k_{bpan}}[\mathrm{PAN}] \quad \text{Eq.3}$$

$$D_{NO_x} = k_{\mathrm{NOOH}}[\mathrm{NO}]_{mod}[\mathrm{OH}] + k_{het}[\mathrm{NO_2}] + \mathrm{k_{fpan}}[\mathrm{NO_2}][\mathrm{CH_3(O)O_2}] + \mathrm{k_{NORO2}}[\mathrm{NO}][\mathrm{RO_2}] + \mathrm{k_{NO2OH}}[\mathrm{NO_2}][\mathrm{OH}] \quad \text{Eq.4}$$

$$\mathrm{P_{OH}} = j_{\mathrm{HONO}}[\mathrm{HONO}] + f \times j_{\mathrm{O^1D}}[\mathrm{O_3}] + k_{\mathrm{NOHO2}}[\mathrm{NO}][\mathrm{HO_2}] + k_{\mathrm{O3HO2}}[\mathrm{O_3}][\mathrm{HO_2}] + j_{H_2O_2}[H_2O_2] + \sum i\{j^i{}_{\mathrm{ROOH}}[\mathrm{ROOH}]_i\} \quad \text{Eq. 5}$$

The HONO budget (Eq. 1 & Eq. 2) was constrained by the measured mixing ratio of NO_2, HONO, OH radicals, the photolysis frequency of HONO, and the HONO flux. The mixing ratio of particulate nitrate ($[\mathrm{pNO_3^-}]$) was derived as the nitrate concentration in the particulate matter $PM_{2.5}$ samples collected during the campaign and measured via ion chromatography, and the mixing ratio of particulate nitrate can be calculated with Eq. 6, as follows:

$$pNO_3^- = \frac{nNO_3^-}{V} \times 10^{-12} \quad \text{Eq. 6}$$

where nNO_3^- (mol) is the amount of nitrate in the $PM_{2.5}$ samples, V is the sampling volume, and 10^{-12} is a unit conversion factor. Due to measurement failures, the mixing ratio of NO had to be calculated in the "Mea." model run as described in model setup section. The previously published reaction rate constant of NO with OH radicals (k_1) and the photolysis frequency of particulate nitrate (j_{pNO3}) were applied[8,21]. The HONO deposition rate was parameterized with the HONO deposition velocity (v_{HONO}) and boundary layer height (BLH). We took the relatively high HONO deposition velocity of 2 cm/s due to the strong turbulence at the NMC site [6,22,23]. The BLH was calculated with the Nozaki method by measuring meteorological parameters of temperature, dew point, and wind speed at 2 m above the ground. The heterogeneous reaction rate of NO_2 (k_{het}) was parameterized using Eq. 7 and Eq. 8 at nighttime (20:00-8:00 (+1 day)) and daytime (8:00-20:00), respectively.

$$k_{het\_N} = \frac{[HONO]_{t2} - [HONO]_{t1}}{\Delta t \times [\overline{NO_2}]} \quad \text{Eq. 7}$$

$$k_{het\_D} = \frac{1}{4} \times \frac{1}{MLH} \times \sqrt{\frac{8RT}{\pi M}} \times \gamma \times \frac{j_{NO2}}{j_{NO2\_noon}} \quad \text{Eq. 8}$$

For nighttime, the NO_2 conversion rate constant was calculated according to the method described previously[2], obtaining an average value of 2.1% [NO_2] h^{-1}; this value is comparable with previous observations of 1.4-2.4% [NO_2] h^{-1} recorded at rural and subrural sites[24–26]. In the daytime, the NO_2 conversion rate constant or uptake coefficient of NO_2 was scaled with the photolysis frequency of NO_2 (j_{NO2}). The term γ is defined as the uptake coefficient of NO_2 under the j_{NO2} reference at noon, j_{NO2_noon}, with an upper-limit value of 6×10^{-5} derived in a previous study[27]. The term $\sqrt{\frac{8RT}{\pi M}}$ (m s^{-1}) is the mean molecular speed of NO_2. MLH is the mixed layer height of HONO;

this value was determined with the photolysis frequency of HONO and turbulent diffusion coefficient(k) with Eq. 9, as follows:

$$\mathrm{MLH} = \sqrt{\frac{2k}{j_{HONO}}} \quad \text{Eq. 9}$$

MLH was calculated at ~ 50 m with an observed HONO lifetime of 10-20 min and k value varying from 1 to 2 m^2/s as determined from flux tower measurements.

Regarding the NO_x budget (Eq. 3 & Eq. 4), HONO-related reactions were calculated with the method described above. PAN-related budget items were calculated with the measured mixing ratio of NO_2, PAN, and the model-generated concentration of peroxyacetyl radicals ($[CH_3CO_3]$). The reaction rate of NO with RO_2 radicals producing organic nitrates ($RONO_2$) was derived as the sum of reactions rates of the model-generated NO with 208 RO_2 species. The reaction rate of NO_2 with OH radicals producing gaseous nitric acid (HNO_3) was constrained with the field-measured concentrations of NO_2 and OH radicals. The photolysis and oxidation of gaseous HNO_3 and $RONO_2$ back to NO_x were minor budget items and thus were not included in this work. All reaction rate constants considered herein were previously published data extracted from the model.

OH radical production (Eq. 5) was calculated to evaluate the perturbation of the external HONO source on the atmospheric oxidative capacity. The budget items were constrained with the field-measured mixing ratio of HONO, O_3, and their photolysis frequencies (j_{HONO}, j_{O^1D}). The reaction rates of HO_2 radicals with NO ($k_{NOHO2}[NO][HO_2]$) and O_3 ($k_{O3HO2}[O_3][HO_2]$), as well as the photolysis of peroxides ($j_{H_2O_2}[H_2O_2] + \sum i\{j^i_{ROOH}[ROOH]_i\}$), were calculated with model-generated mixing ratio of NO, HO_2, H_2O_2 and peroxides and were extracted from the model.

Model description. A zero-dimensional photochemical box model based on the Master Chemical Mechanism (MCM)[29] was used to help calculate the budgets of HONO, NO_x and OH and evaluate the impact of external cycling on HONO, NO_x and OH radicals with HONO as the

intermediate tracer. The mechanism consisted of 11152 gas-phase reactions extracted from the website (MCM v3.3.1, http://mcm.leeds.ac.uk/MCM), including all inorganic chemistry reactions and organic chemistry reactions related to VOCs and OVOCs measurements. The heterogeneous conversion of NO_2 and deposition of HONO were also included in the chemical mechanism with the parameterization methods described above.

Two model runs were designed and conducted. The control model run (referred to herein as "Mea.") was constrained by the diurnal variations of parameters listed in Table S2. The sensitive model run ("Base") was constrained with all parameters as in "Mea." model except HONO, NO_2 and OH radicals. The model setup was fully described in Table S2. The comparison of these two model runs provided evidence for the perturbation of external HONO on NO_x and OH radicals. Each model was initialized with inputs from the first measurement day and spun up for days, before the concentrations and budgets of HONO, NO_x and OH radicals were extracted and analyzed on the third day.

Results and Discussion

To identify the external cycling in polar areas, several key arguments, such as the distributions and budgets of HONO and NO_x, mechanism analyses and atmospheric perturbations of external cycling, have been comprehensively discussed in various studies lasting from the 1990s to the present[11–16,28–31]. The polar scenario suggests a revision of atmospheric photochemistry by the external cycling mechanism within the snowpack[11,16]. Specifically, an external source of nitrate photolysis on snow/ice surfaces promotes HONO and NO_x abundances and increases HO_x to levels even exceeding those found in tropical marine boundaries[15]. Herein, we follow this lead to explore the scientific questions raised above.

Distributions of HONO, NO_x and the PSS HONO/NO_x ratio

The hourly mixing ratio of HONO ranged from 7 to 94 pptv from 2 – 20 May (Figure. S1 (a)). The average mixing ratio of HONO at this pristine alpine site was 30 (±13, 1σ) pptv. Our HONO observations are comparable with other measurements recorded in terrestrial background environments, such as the value of 46 pptv observed at the summit of Whiteface Mountain[32], that of 32 pptv measured in a boreal forest[33], and that of 35 pptv measured at a background coastal site in Cyprus[34], while it is slightly higher than the measurements of 8-35 pptv recorded in polar areas[11,13,31,35,36]. Higher HONO mixing ratio values were frequently found in the daytime observations compared to those in the nighttime observations, in contrast to the relatively fast photolysis with a photolysis rate constant of 1–1.6 $\times 10^{-3}$ s^{-1}. Occasionally, spikes occurred on several nights along with spikes in the NO_2 mixing ratio, suggesting the influence of the local combustion of cow dung cakes and emissions from visiting vehicles.

The mixing ratios of NO_2 ranged from 20 to 620 pptv, with high values occurring in narrow spikes (Figure. S1 (b)). The time durations comprising these NO_2 spike occurrences consisted of ~7.5% of the whole measurement period. A small discrepancy between the average mixing ratio of 143 (±100, 1σ) pptv and the median value of 119 pptv was also observed. We therefore concluded that occasional emissions do not significantly raise the pollution level of this pristine site. For the mixing ratio of NO, we projected a daytime average value of 34 (±26, 1σ) pptv and a nighttime value near zero due to titration by ca. 50 ppb of O_3. These mixing ratios of NO_x were comparable with those measured at 100-300 pptv in terrestrial background sites[32–34] but were slightly higher than the tens of pptv observed in polar regions[12,15,35].

The HONO/NO_x ratios varied from 0.03 to 1 during this field campaign, with mean and median values of 0.26 (±0.18, 1σ) and 0.20, respectively (Figure S1 (c)). The HONO/NO_x ratio was substantially higher than the 0.006-0.05 ratios observed in urban sites[5] but was comparable with

the 0.06-0.53 values observed in polar areas and terrestrial background sites[11–14,16,33–35,37,38]. Relatively high HONO/NO_x ratios were frequently observed in daytime than nighttime, with peak values mostly occurring around noon.

The measured diurnal patterns of HONO, NO_x and the HONO/NO_x ratio are shown in black line in Figure 1. A bridge-shaped diurnal pattern of HONO was characterized with a noontime (12:00-13:00) maximum of 40 pptv and a nighttime (20:00-8:00) minimum of 22 pptv; this pattern was consistent with the corresponding time-series observations on most days. The diurnal pattern of NO_x was characterized with relatively high values of 190 (±38, 1σ) pptv at night and slightly lower values of 135 (±21, 1σ) pptv during the day on average. Bridge-shaped diurnal pattern was also observed for the HONO/NO_x ratio. The average HONO/NO_x ratio was 0.20(±0.03, 1σ) throughout the night while averaged at 0.31(±0.06, 1σ) in the daytime. Contradictory to the measurements, obvious U-shape diurnal patterns of HONO, NO_x and HONO/NO_x radio were predicted with the "Base" model run, the chemical model simulations performed with a simple internal cycling mechanism (Figure 1., red dash line). The predicted HONO concentration was averaged at 3.5 (±1.2, 1σ) pptv in the nighttime and 1 (±0.9, 1σ) pptv in the daytime. NO_x concentrations were projected at 17 (±8, 1σ) pptv in the daytime and 38 (±2, 1σ) pptv at night on average. HONO/NO_x ratio was averaged at 0.07 (±0.03, 1σ) throughout the day, and at 0.05 (±0.007, 1σ) in the daytime.

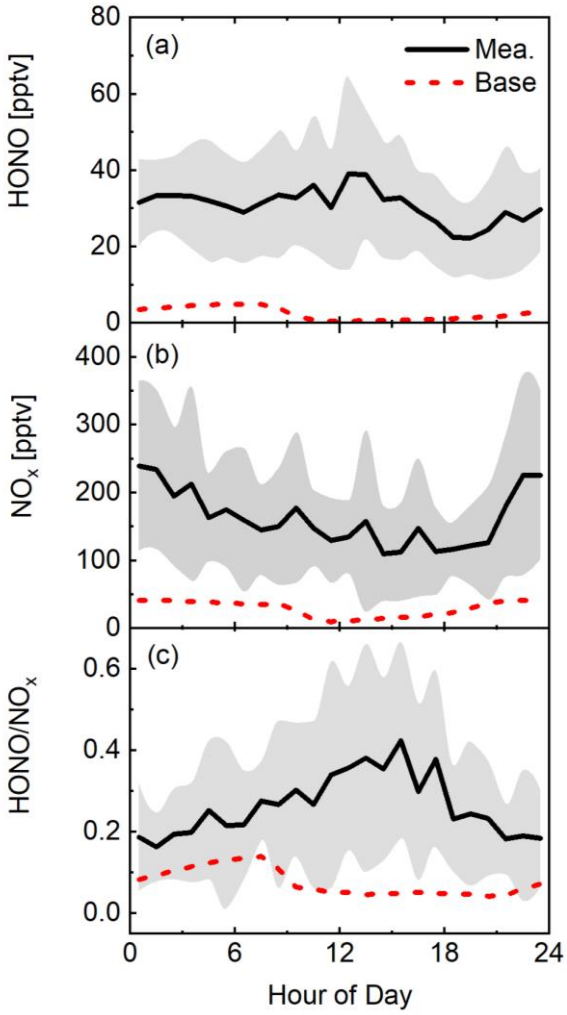

Figure 1. Diurnal patterns of (a) HONO, (b) NO_x, and (c) HONO/NO_x ratio. The "Mea." model results are shown as a black line, with the gray shaded area representing the variation (±1σ). The "Base" model predictions are shown as red dashed lines.

Here, we conclude that external cycling prevails and dominates at the background site based on the distribution patterns of HONO, NO_x and the HONO/NO_x ratio. First, the "Base" model run underestimates the HONO and NO_x observations by 90% and 80%, respectively (Figure 1(a) & (b)), suggesting that the internal cycling mechanisms could only explain a minor part of HONO and NO_x abundance. Second, a PSS HONO/NO_x ratio, i.e. HONO/NO_x ratio in the daytime, of

0.05 was predicted in the "Base" model run in the daytime; this value was substantially lower than the observed PSS HONO/NO_x ratio of 0.31(±0.06, 1σ). The high HONO/NO_x ratio further suggested that internal cycling was not sufficiently strong to sustain daytime HONO concentrations. Elevated HONO/NO_x ratio was attributed to the photosensitization of NO_2 recorded on the ground surface in previous field measurements[35]. However, here, we took the upper-limit NO_2 heterogenous conversion rate of 6×10^{-5} derived in previous field campaigns, though this value could still not explain the observed HONO/NO_x ratio, suggesting a missing source of HONO from non-NO_x precursors, i.e., an external source. In addition, no correlation between the mixing ratios of HONO and NO_2 was observed ($R^2<0.1$), implying that the distributions of HONO and NO_x are not controlled by their internal cycling. Third, the bridge-shaped diurnal pattern of HONO and the relatively stable diurnal pattern of NO_x against their photolysis and oxidative losses could only be reconciled by a mutual source of HONO and NO_x, i.e., an external source. This external source should be scaled by temperature or solar radiation to sustain the noontime HONO and NO_2 observations. Last but not least, the proxy mechanisms of external sources discussed in previous literature are reasonable, as they produce HONO and NO_x at a high production ratio and are scaled with either temperature or solar radiation. First, nitrate photolysis has been extrapolated to ambient surfaces, such as tree leaves, urban grimes, and aerosol surfaces, with a HONO/NO_x production ratio range of 0.4-33[21,39–41]. The light-related and surface-catalyzed characteristics of this process make it a potential mechanism at this background site on the Tibetan Plateau. Nitrification and/or denitrification processes in surface soils where nitrate or ammonium is available as a HONO precursor are another proven external source[42,43]. Soil emissions of HONO have been observed in both fertile and barren soils, such as those in forests, grasslands, and deserts, both in the field and laboratory, supporting such an external HONO source

as a universal source[42]. Overall, the distribution patterns of HONO, NO_x and HONO/NO_x indicate the dominant role of this external source on the HONO budget.

Chemical budget of HONO

Our measurement constraint on the HONO budget allowed us to quantify the internal and external cycling routes of HONO and NO_x. The HONO budget is shown in Figure 2. At night, HONO was produced at a rate of 4 pptv h^{-1} through the heterogeneous conversion of NO_2. This rate was not only small but may also have been offset by HONO deposition at a magnitude of 3 pptv h^{-1}. The nighttime budget calculation was in line with our observation of stable HONO throughout the night, suggesting that no or only minor nighttime accumulation occurs from heterogeneous reactions of NO_2 on the ground surface. In the daytime, the homogeneous reaction between NO and OH radicals produces HONO at an average rate of 3 pptv h^{-1}; this rate is negligible compared to the overall HONO source budget of 130 pptv h^{-1}. The heterogeneous conversion of NO_2 on the ground is accelerated by solar radiation. Given an upper limit of the noontime uptake coefficient of 6×10^{-5}, the daytime average rate of 25 pptv h^{-1} was calculated. Although the upper limit of the uptake coefficient was taken into consideration here[10,27,44], the conversion of NO_2 was still only one-sixth of the daytime HONO source budget. Here, we evaluated the 30 pptv h^{-1} rate produced by internal sources in the daytime and projected its contribution to the overall HONO budget to be ca. 23%. The external HONO source thus accounted for at least 77% of the HONO source budget in the daytime and an average daytime HONO production rate of 100 pptv h^{-1}.

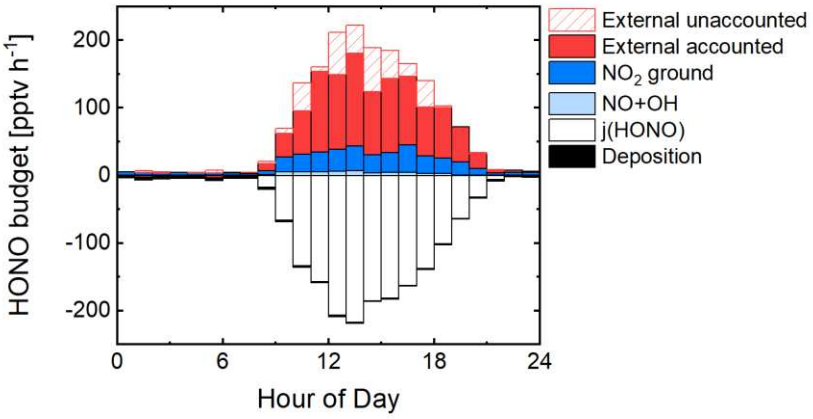

Figure 2. Chemical budget terms of HONO as evaluated by the "Mea." model. HONO deposition is shown with the black bar; photolysis (j(HONO)) is shown with the white bar; the reaction of NO with OH radicals (NO+OH) is shown with the light blue bar; and the heterogenous conversion of NO_2 on ground surfaces (NO_2 ground) is shown with the blue bar. The external sources accounted for by surface fluxes and particulate nitrate photolysis (External accounted) are shown with red bars. The remaining external source (External unaccounted) is shown with the red line bars.

Surface flux measurements of HONO provided a constraint on external cycling. During the field campaign, an average daytime HONO flux of 0.02 nmol m^{-2} s^{-1} was measured (Figure S1 (g)). Assuming an MLH of 50 m described in Materials and Methods, the surface HONO flux was converted into an in situ HONO source rate of ca. 65 pptv h^{-1}. The upper limit of photo-enhanced heterogeneous conversion of NO_2 on the ground surface was estimated to be 25 pptv h^{-1}, suggesting an external source accounting for at least the remainder of 40 pptv h^{-1}. Both soil emissions and the surface-catalytic photolysis of nitrate on ground surfaces are candidates for this external source.

The response of the HONO flux peak to precipitation with a delay of one day might be attributed to the soil activation mechanism, implying the dominating role of soil emissions (Figure S1 (g)).

An in situ external HONO source from the photolysis of particulate nitrate cannot be ruled out. The photolysis of particulate nitrate has been found to be enhanced by 1-3 orders of magnitude compared to that of gaseous nitric acid[21,40]. We took the photolysis frequency of 1.3×10^{-4} s^{-1} to estimate the HONO production rate via particulate nitrate photolysis in this study, which is the mean value derived from HONO production via particulate nitrate photolysis experiments with particulates collected over a variety of various environments[21]. The mean nitrate concentration of $PM_{2.5}$ samples collected during the campaign was 110 pptv. We therefore estimated an in situ HONO production rate of approximately 35 pptv h^{-1} in the daytime.

All these external sources summed up to 75 pptv h^{-1}, 25% less than the total external source of 100 pptv h^{-1} derived from the HONO budget analysis. This discrepancy was, however, within the measurement uncertainties. Specifically, the measurement uncertainties were determined to be 25% for HONO and 35% for the HONO flux. Uncertainties also arose from the evaluation of external HONO source candidates, but these uncertainties are difficult to quantify. First, to evaluate the HONO source from the flux measurements, we assumed a uniform distribution of HONO in the 50-m mixed layer. However, with a noontime solar radiation measurement of 1700 W m^{-2} and an average wind speed of 4 m s^{-1}, rapid vertical mixing of HONO should be expected. Therefore, the HONO budget item would be very sensitive to the MLH evaluation. Second, in situ HONO production from particulate nitrate photolysis is heavily dependent on the photolysis frequencies observed in different environments[21], which might also vary in the pristine environment of the NMC site.

Despite these uncertainties, our HONO budget evaluation provides evidence that both soil emissions and the surface-catalytic photolysis of nitrate are potential proxy mechanisms representing the unidentified external source. However, the large uncertainties hinder the separation of the contributions of these two proxy mechanisms. Further precise quantification measurements of the two external source candidates in the mixed layer, combined with a chemical transport model analysis, are thus encouraged.

Perturbation of NO_x and OH radicals

External sources of HONO are also sources of NO_x because HONO quickly photolyzes, producing NO. Therefore, we propose the occurrence of external cycling routes of NO_x with HONO as an intermediate tracer. External cycling further promotes OH radical production directly via HONO photolysis and indirectly via OH recycling routes, such as the reaction of NO with HO_2 radicals. Our model evaluates the perturbation of this external source on the distributions and budgets of NO_x and OH radicals.

The model results underline HONO as a critical intermediate to NO_x. Specifically, in the "Mea." model run constrained by our measurements, 100 pptv h^{-1} of net NO_x production (HONO net $= j_{HONO}[HONO] - k_1[NO]_{mod}[OH] - k_{het}[NO_2]$) was determined to occur via the photolysis of external HONO. The photolysis of external HONO dominated the chemical production of NO_x in this pristine environment. Nevertheless, the formation of PAN, HNO_3 and $RONO_2$ provide NO_x sinks at this site. A net loss of NO_x to PAN (PAN net $= k_{bpan}[PAN] - k_{fpan}[NO_2][CH_3CO_3 \cdot]$) at a rate of 90 pptv h^{-1} was predicted in the model. High abundances of NO_2 and CH_3CO_3 radicals promote the reaction of NO_2 with CH_3CO_3 radicals to a rate of 110 pptv h^{-1}, while the low temperatures in this alpine site suppress the thermal decomposition of PAN to a rate of 20 pptv h^{-1}. When further seeking the precursors of CH_3CO_3 radicals, we found acetaldehyde at a

concentration of 1 ppb at this site; however, the source of this acetaldehyde is not yet clear. Relatively slow losses of NO_x to $RONO_2$ and HNO_3 were projected in the model at rates of 6 pptv h^{-1} and 9 pptv h^{-1}, respectively. The chemical budget of NO_x is imbalanced, with an unaccounted source in early morning and unaccounted sink in the afternoon. There are two possible explanations for the imbalance. First, direct production of NO_x in external cycling was not included in our budget analyses. Second, as discussed for HONO above, vertical mixing of NO_x into a higher layer of air masses is a potential sink of NO_x. However, with the mechanisms currently considered, we still conclude external HONO as a precursor to NO_x and HONO as the intermediate tracer of the external cycling, by the discrepancy between the "Mea" and "Base" model results (Figure 3(b)). In the "Base" model run in which only internal cycling was included, "HONO net" was nearly zero in the daytime because HONO photolysis was offset by NO_x-related reactions and no net NO_x was produced.

OH production is greatly promoted as a result of external cycling. As shown in Figure 3 (c), the OH production rate was doubled in the daytime in the "Mea." model run compared to that in the "Base" run. Of the enhancements, 54% and 23% could be attributed to the reaction of NO with HO_2 radicals and to the photolysis of HONO, respectively. The enhancement of OH production resulted in an elevated mixing ratio of OH radicals. The measured mixing ratio of OH radicals was 2.25 times higher than that predicted in the "Base" model run in the daytime, with average values of 2.67×10^6 molecule/cm^3 and 1.49×10^6 molecule/cm^3, respectively (Figure S2). These results imply an underestimation of the atmospheric oxidative capacity at this background site if only the internal cycling of HONO and NO_x is considered.

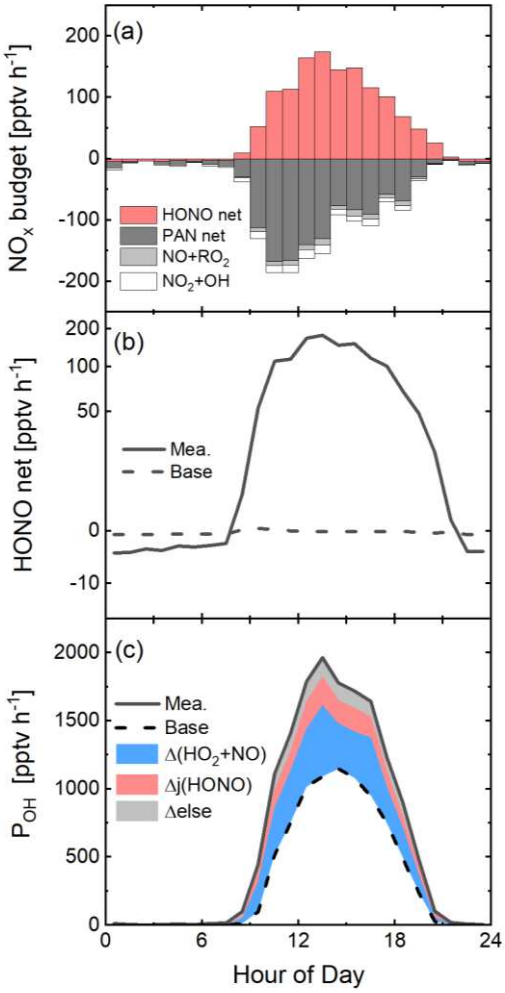

409

410 **Figure 3.** (a) NO_x budget calculated in the "Mea." model run. $\mathrm{HONO\ net} = j_{HONO}[HONO] -$

411 $k_1[NO]_{mod}[OH] - k_{het}[NO_2]$ and $\mathrm{PAN\ net} = k_{bpan}[PAN] - k_{fpan}[NO_2][CH_3CO_3 \cdot]$; (b)

412 "HONO net" calculated in two model runs. The rate predicted with the "Mea." model is shown as

413 a solid line, while that predicted with the "Base" model is shown as a dashed line. (c) OH

414 production rates calculated in two model runs. The rate predicted with the "Mea." model is shown

415 as a solid line, while that predicted with the "Base" model is shown as a dashed line. The blue, red,

416 and gray shaded areas represent the enhancement of the OH production rate via the reaction of NO

417 with HO_2 radicals, HONO photolysis and the reactions of the model-generated species.

Environmental implications

High PSS HONO/NO_x ratios are prevalently observed in pristine areas[15,32,33,38]. Here, we summarize the daytime HONO and NO_x concentrations measured in the background atmosphere and compare them with those measured in the urban atmosphere (Figure 4 & Table S3). In the urban atmosphere, the PSS HONO/NO_x ratio values are scattered around approximately 0.02, thus strengthening that the internal cycling chemistry of HONO and NO_x dominates in such environments[5]. However, the PSS HONO/NO_x ratios measured in the background environments range from 0.06 to 0.77. The fitting PSS HONO/NO_x ratio of 0.17 was derived for the background atmosphere; this ratio is significantly higher than that obtained for urban observations. This finding is indicative of external cycling having taken over in pristine atmosphere, while internal cycling was still inclusive.

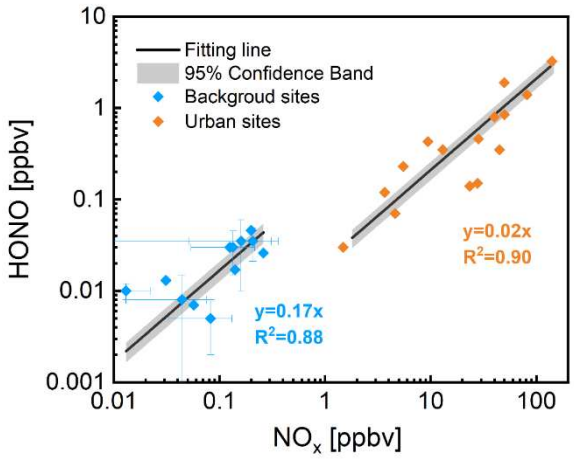

Figure 4. Distributions of HONO against NO_x observed in the daytime in background (blue) and urban (orange) sites. The solid lines and gray shaded areas are the fitting lines and 95% confidence bands, respectively, for the two scenarios. The linear fitting results are shown in blue and orange for background and urban sites, respectively, with the slope representing PSS HONO/NO_x.

By deducing a high HONO/NO_x ratio as a sufficient condition for external cycling, we validate the prevalence of external cycling in general background atmosphere. The great perturbation of external cycling on the budgets of NO_x and OH radicals was also validated. Underappreciating the external cycling mechanism is therefore a major flaw of our current understanding of the reactive nitrogen cycling process and atmospheric oxidative capacity in background terrestrial environments.

ASSOCIATED CONTENT

Supporting Information.

The following files are available free of charge.

HONO _ intermediate tracer _ SI .pdf

AUTHOR INFORMATION

Corresponding Author

Chunxiang Ye - State Key Joint Laboratory for Environmental Simulation and Pollution Control, College of Environmental Sciences and Engineering, Peking University, Beijing, 100871, China.

Email: c.ye@pku.edu.cn

Authors

Jianshu Wang - State Key Joint Laboratory for Environmental Simulation and Pollution Control, College of Environmental Sciences and Engineering, Peking University, Beijing, 100871, China.

Yingjie Zhang - State Key Joint Laboratory for Environmental Simulation and Pollution Control, College of Environmental Sciences and Engineering, Peking University, Beijing, 100871, China; School of Ecology and Nature Conservation, Beijing Forestry University, Beijing, 100083, China.

Chong Zhang - State Key Joint Laboratory for Environmental Simulation and Pollution Control, College of Environmental Sciences and Engineering, Peking University, Beijing, 100871, China.

Yaru Wang - State Key Joint Laboratory for Environmental Simulation and Pollution Control, College of Environmental Sciences and Engineering, Peking University, Beijing, 100871, China.

Jiacheng Zhou - Laboratory of Atmospheric Physico-Chemistry, Hefei Institutes of Physical Science Anhui Institute of Optics and Fine Mechanics, Chinese Academy of Sciences, Hefei, 230031, Anhui, China.

Lisa K. Whalley - School of Chemistry, University of Leeds, Leeds, LS2 9JT, UK.

Eloise J. Slater - School of Chemistry, University of Leeds, Leeds, LS2 9JT, UK.

Joanna E. Dyson - School of Chemistry, University of Leeds, Leeds, LS2 9JT, UK; British Antarctic Survey, Cambridge, CB3 0ET, UK

Wanyun Xu - Chinese Academy of Meteorological Science, Institute of Atmospheric Composition, Beijing, 100081, China.

Peng Cheng - Institute of Mass Spectrometry and Atmospheric Environment, Jinan University, Guangzhou, 510632, China

Baobin Han - Institute of Mass Spectrometry and Atmospheric Environment, Jinan University, Guangzhou, 510632, China

Lifan Wang – State Key Joint Laboratory for Environmental Simulation and Pollution Control, College of Environmental Sciences and Engineering, Peking University, Beijing, 100871, China.

Xuena Yu - State Key Joint Laboratory for Environmental Simulation and Pollution Control, and College of Environmental Sciences and Engineering, Peking University, Beijing, 100871, China.

Youfeng Wang - State Key Joint Laboratory for Environmental Simulation and Pollution Control, College of Environmental Sciences and Engineering, Peking University, Beijing, 100871, China.

Robert Woodward-Messy - State Key Joint Laboratory for Environmental Simulation and Pollution Control, College of Environmental Sciences and Engineering, Peking University, Beijing, 100871, China.

Weili Lin – Key Laboratory of Ecology and Environment in Minority Areas, Minzu University of China, National Ethnic Affairs Commission, Beijing 100081, China

Weixiong Zhao - Laboratory of Atmospheric Physico-Chemistry, Hefei Institutes of Physical Science Anhui Institute of Optics and Fine Mechanics, Chinese Academy of Sciences, Hefei, 230031, Anhui, China.

Limin Zeng - State Key Joint Laboratory for Environmental Simulation and Pollution Control, College of Environmental Sciences and Engineering, Peking University, Beijing, 100871, China.

Zhiqiang Ma - China Meteorological Administration Beijing Institute of Urban Meteorology, Beijing, 100089, China.

Dwayne E. Heard - School of Chemistry, University of Leeds, Leeds, LS2 9JT, UK.

Author Contributions

J.W. and C.Y. design the research, interpreted the data, and wrote the manuscript. J.W., Y.Z., C.Z., Y.W., J.Z., L.K.W., E.J.S., J.E.D., W.X., and P.C. conducted the measurements. J.W., Y.W., and R.W.M conducted the model simulations. The manuscript was written through contributions of all authors. All authors have given approval to the final version of the manuscript.

Funding Sources

This work was supported by the National Natural Science Foundation of China (Grants Nos. 42175120, 41875151, and 42105110), Second Tibetan Plateau Scientific Expedition and Research Program (2019QZKK060604).

Notes

The authors declare no competing financial interest.

ACKNOWLEDGMENT

We thank all researchers involved in the @Tibet 2019 campaign from Peking University, Hefei Institutes of Physical Science Anhui Institute of Optics and Fine Mechanics of Chinese Academy of Sciences, Chinese Academy of Meteorological Science, University of Leeds, University of Science and Technology of China.

REFERENCES

(1) Alicke, B.; Platt, U.; Stutz, J. Impact of Nitrous Acid Photolysis on the Total Hydroxyl Radical Budget during the Limitation of Oxidant Productioh/Pianura Padana Produzione Di Ozono Study in Milan. *Journal of Geophysical Research Atmospheres* **2002**, *107* (22). https://doi.org/10.1029/2000JD000075.

(2) Alicke, B.; Geyer, A.; Hofzumahaus, A.; Holland, F.; Konrad, S.; Pätz, H. W.; Schäfer, J.; Stutz, J.; Volz-Thomas, A.; Platt, U. OH Formation by HONO Photolysis during the BERLIOZ Experiment. *Journal of Geophysical Research: Atmospheres* **2003**, *108* (4). https://doi.org/10.1029/2001jd000579.

(3) Acker, K.; Febo, A.; Trick, S.; Perrino, C.; Bruno, P.; Wiesen, P.; Möller, D.; Wieprecht, W.; Auel, R.; Giusto, M.; Geyer, A.; Platt, U.; Allegrini, I. Nitrous Acid in the Urban Area of Rome. *Atmos Environ* **2006**, *40* (17), 3123–3133. https://doi.org/10.1016/j.atmosenv.2006.01.028.

(4) Kurtenbach, R.; Becker, K. H.; Gomes, J. A. G.; Kleffmann, J.; Orzer, J. C. L.; Spittler, M.; Wiesen, P.; Ackermann, R.; Geyer, A.; Platt, U. *Investigations of Emissions and Heterogeneous Formation of HONO in a Road Traffic Tunnel*; 2001; Vol. 35.

(5) Elshorbany, Y. F.; Steil, B.; Brühl, C.; Lelieveld, J. Impact of HONO on Global Atmospheric Chemistry Calculated with an Empirical Parameterization in the EMAC Model. *Atmos Chem Phys* **2012**, *12* (20), 9977–10000. https://doi.org/10.5194/acp-12-9977-2012.

(6) Stutz, J.; Alicke, B.; Neftel, A. Nitrous Acid Formation in the Urban Atmosphere: Gradient Measurements of NO2 and HONO over Grass in Milan, Italy. *Journal of Geophysical Research Atmospheres* **2002**, *107* (22). https://doi.org/10.1029/2001JD000390.

(7) Kleffmann, J. Daytime Sources of Nitrous Acid (HONO) in the Atmospheric Boundary Layer. *ChemPhysChem* **2007**, *8* (8), 1137–1144. https://doi.org/10.1002/cphc.200700016.

(8) Atkinson, R.; Baulch, D. L.; Cox, R. A.; Crowley, J. N.; Hampson, R. F.; Hynes, R. G.; Jenkin, M. E.; Rossi, M. J.; Troe, J. Evaluated Kinetic and Photochemical Data for Atmospheric Chemistry: Volume I - Gas Phase Reactions of O_x, HO_x, NO_x and SO_x Species. *Atmos Chem Phys* **2004**, *4* (6), 1461–1738. https://doi.org/10.5194/acp-4-1461-2004.

(9) Xu, Z.; Wang, T.; Wu, J.; Xue, L.; Chan, J.; Zha, Q.; Zhou, S.; Louie, P. K. K.; Luk, C. W. Y. Nitrous Acid (HONO) in a Polluted Subtropical Atmosphere: Seasonal Variability, Direct Vehicle Emissions and Heterogeneous Production at Ground Surface. *Atmos Environ* **2015**, *106* (x), 100–109. https://doi.org/10.1016/j.atmosenv.2015.01.061.

(10) Stemmler, K.; Ammann, M.; Donders, C.; Kleffmann, J.; George, C. Photosensitized Reduction of Nitrogen Dioxide on Humic Acid as a Source of Nitrous Acid. *Nature* **2006**, *440* (7081), 195–198. https://doi.org/10.1038/nature04603.

(11) Zhou, X.; Beine, H. J.; Honrath, R. E.; Fuentes, J. D.; Simpson, W.; Shepson, P. B.; Bottenheim, J. W. Snowpack Photochemical Production of HONO: A Major Source of OH in the Arctic Boundary Layer in Springtime. *Geophys Res Lett* **2001**, *28* (21), 4087–4090. https://doi.org/10.1029/2001GL013531.

(12) Beine, H. J.; Honrath, R. E.; Dominé, F.; Simpson, W. R.; Fuentes, J. D. NOx during Background and Ozone Depletion Periods at Alert: Fluxes above the Snow Surface. *Journal of Geophysical Research Atmospheres* **2002**, *107* (21). https://doi.org/10.1029/2002JD002082.

(13) Davis, D.; Chen, G.; Buhr, M.; Crawford, J.; Lenschow, D.; Lefer, B.; Shetter, R.; Eisele, F.; Mauldin, L.; Hogan, A. South Pole NOx Chemistry: An Assessment of Factors Controlling Variability and Absolute Levels. *Atmos Environ* **2004**, *38* (32), 5375–5388. https://doi.org/10.1016/j.atmosenv.2004.04.039.

(14) Dibb, J. E.; Gregory Huey, L.; Slusher, D. L.; Tanner, D. J. Soluble Reactive Nitrogen Oxides at South Pole during ISCAT 2000. *Atmos Environ* **2004**, *38* (32), 5399–5409. https://doi.org/10.1016/j.atmosenv.2003.01.001.

(15) Yang, J.; Honrath, R. E.; Peterson, M. C.; Dibb, J. E.; Sumner, A. L.; Shepson, P. B.; Frey, M.; Jacobi, H.-W.; Swanson, A.; Blake, N. *Impacts of Snowpack Emissions on Deduced Levels of OH and Peroxy Radicals at Summit, Greenland*; 2002; Vol. 36.

(16) Honrath, R. E.; Lu, Y.; Peterson, M. C.; Dibb, J. E.; Arsenault, M. A.; Cullen, N. J.; Steffen, K. Vertical Fluxes of NOx, HONO, and HNO3 above the Snowpack at Summit, Greenland. *Atmos Environ* **2002**, *36* (15–16), 2629–2640. https://doi.org/10.1016/S1352-2310(02)00132-2.

(17) Jacobi, H. W.; Hilker, B. A Mechanism for the Photochemical Transformation of Nitrate in Snow. *J Photochem Photobiol A Chem* **2007**, *185* (2–3), 371–382. https://doi.org/10.1016/j.jphotochem.2006.06.039.

(18) Heland, J.; Kleffmann, J.; Kurtenbach, R.; Wiesen, P. A New Instrument to Measure Gaseous Nitrous Acid (HONO) in the Atmosphere. *Environ Sci Technol* **2001**, *35* (15), 3207–3212. https://doi.org/10.1021/es000303t.

(19) Fang, B.; Zhao, W.; Xu, X.; Zhou, J.; Ma, X.; Wang, S.; Zhang, W.; Venables, D. S.; Chen, W. Portable Broadband Cavity-Enhanced Spectrometer Utilizing Kalman Filtering: Application to Real-Time, in Situ Monitoring of Glyoxal and Nitrogen Dioxide. *Opt Express* **2017**, *25* (22), 26910. https://doi.org/10.1364/OE.25.026910.

(20) Wang, M.; Zeng, L.; Lu, S.; Shao, M.; Liu, X.; Yu, X.; Chen, W.; Yuan, B.; Zhang, Q.; Hu, M.; Zhang, Z. Development and Validation of a Cryogen-Free Automatic Gas Chromatograph System (GC-MS/FID) for Online Measurements of Volatile Organic Compounds. *Analytical Methods* **2014**, *6* (23), 9424–9434. https://doi.org/10.1039/c4ay01855a.

(21) Ye, C.; Zhang, N.; Gao, H.; Zhou, X. Photolysis of Particulate Nitrate as a Source of HONO and NOx. *Environ Sci Technol* **2017**, *51* (12), 6849–6856. https://doi.org/10.1021/acs.est.7b00387.

(22) Laufs, S.; Cazaunau, M.; Stella, P.; Kurtenbach, R.; Cellier, P.; Mellouki, A.; Loubet, B.; Kleffmann, J. Diurnal Fluxes of HONO above a Crop Rotation. *Atmos Chem Phys* **2017**, *17* (11), 6907–6923. https://doi.org/10.5194/acp-17-6907-2017.

(23) Trebs, I.; Lara, L. L.; Zeri, L. M. M.; Gatti, L. v; Artaxo, P.; Dlugi, R.; Slanina, J.; Andreae, M. O.; Meixner, F. X. *Dry and Wet Deposition of Inorganic Nitrogen Compounds to a Tropical Pasture Site (Rondônia, Brazil)*; 2006; Vol. 6.

(24) Su, H.; Cheng, Y. F.; Cheng, P.; Zhang, Y. H.; Dong, S.; Zeng, L. M.; Wang, X.; Slanina, J.; Shao, M.; Wiedensohler, A. Observation of Nighttime Nitrous Acid (HONO) Formation at a Non-Urban Site during PRIDE-PRD2004 in China. *Atmos Environ* **2008**, *42* (25), 6219–6232. https://doi.org/10.1016/j.atmosenv.2008.04.006.

(25) Sörgel, M.; Regelin, E.; Bozem, H.; Diesch, J. M.; Drewnick, F.; Fischer, H.; Harder, H.; Held, A.; Hosaynali-Beygi, Z.; Martinez, M.; Zetzsch, C. Quantification of the Unknown HONO Daytime Source and Its Relation to NO2. *Atmos Chem Phys* **2011**, *11* (20), 10433–10447. https://doi.org/10.5194/acp-11-10433-2011.

(26) Li, X.; Brauers, T.; Häseler, R.; Bohn, B.; Fuchs, H.; Hofzumahaus, A.; Holland, F.; Lou, S.; Lu, K. D.; Rohrer, F.; Hu, M.; Zeng, L. M.; Zhang, Y. H.; Garland, R. M.; Su, H.; Nowak, A.; Wiedensohler, A.; Takegawa, N.; Shao, M.; Wahner, A. Exploring the Atmospheric Chemistry of Nitrous Acid (HONO) at a Rural Site in Southern China. *Atmos Chem Phys* **2012**, *12* (3), 1497–1513. https://doi.org/10.5194/acp-12-1497-2012.

(27) Wong, K. W.; Tsai, C.; Lefer, B.; Grossberg, N.; Stutz, J. Modeling of Daytime HONO Vertical Gradients during SHARP 2009. *Atmos Chem Phys* **2013**, *13* (7), 3587–3601. https://doi.org/10.5194/acp-13-3587-2013.

(28) Barbero, A.; Savarino, J.; Grilli, R.; Blouzon, C.; Picard, G.; Frey, M. M.; Huang, Y.; Caillon, N. New Estimation of the NO_x Snow-Source on the Antarctic Plateau. *Journal of Geophysical Research: Atmospheres* **2021**, *126* (20). https://doi.org/10.1029/2021JD035062.

(29) Ianniello, A.; Spataro, F.; Salvatori, R.; Valt, M.; Nardino, M.; Björkman, M. P.; Esposito, G.; Montagnoli, M. Air-Snow Exchange of Reactive Nitrogen Species at Ny-Ålesund, Svalbard (Arctic). *Rendiconti Lincei* **2016**, *27*, 33–45. https://doi.org/10.1007/s12210-016-0536-4.

(30) Honrath, R. E.; Peterson, M. C.; Guo, S.; Dibb, J. E.; Shepson, P. B.; Campbell, B. Evidence of NO x Production within or upon Ice Particles in the Greenland Snowpack. *Geophys Res Lett* **1999**, *26* (6), 695–698. https://doi.org/10.1029/1999GL900077.

(31) Legrand, M.; Preunkert, S.; Frey, M.; Bartels-Rausch, T.; Kukui, A.; King, M. D.; Savarino, J.; Kerbrat, M.; Jourdain, B. Large Mixing Ratios of Atmospheric Nitrous Acid (HONO) at Concordia (East Antarctic Plateau) in Summer: A Strong Source from Surface Snow? *Atmos Chem Phys* **2014**, *14* (18), 9963–9976. https://doi.org/10.5194/acp-14-9963-2014.

(32) Zhou, X.; Huang, G.; Civerolo, K.; Roychowdhury, U.; Demerjian, K. L. Summertime Observations of HONO, HCHO, and O3 at the Summit of Whiteface Mountain, New York. *Journal of Geophysical Research Atmospheres* **2007**, *112* (8), 1–13. https://doi.org/10.1029/2006JD007256.

(33) Oswald, R.; Ermel, M.; Hens, K.; Novelli, A.; Ouwersloot, H. G.; Paasonen, P.; Petäjä, T.; Sipilä, M.; Keronen, P.; Bäck, J.; Königstedt, R.; Hosaynali Beygi, Z.; Fischer, H.; Bohn, B.; Kubistin, D.; Harder, H.; Martinez, M.; Williams, J.; Hoffmann, T.; Trebs, I.; Sörgel, M. A Comparison of HONO Budgets for Two Measurement Heights at a Field Station within the Boreal Forest in Finland. *Atmos Chem Phys* **2015**, *15* (2), 799–813. https://doi.org/10.5194/acp-15-799-2015.

(34) Meusel, H.; Kuhn, U.; Reiffs, A.; Mallik, C.; Harder, H.; Martinez, M.; Schuladen, J.; Bohn, B.; Parchatka, U.; Crowley, J. N.; Fischer, H.; Tomsche, L.; Novelli, A.; Hoffmann, T.; Janssen, R. H. H.; Hartogensis, O.; Pikridas, M.; Vrekoussis, M.; Bourtsoukidis, E.; Weber,

B.; Lelieveld, J.; Williams, J.; Pöschl, U.; Cheng, Y.; Su, H. Daytime Formation of Nitrous Acid at a Coastal Remote Site in Cyprus Indicating a Common Ground Source of Atmospheric HONO and NO. *Atmos Chem Phys* **2016**, *16* (22), 14475–14493. https://doi.org/10.5194/acp-16-14475-2016.

(35) Villena, G.; Wiesen, P.; Cantrell, C. A.; Flocke, F.; Fried, A.; Hall, S. R.; Hornbrook, R. S.; Knapp, D.; Kosciuch, E.; Mauldin, R. L.; McGrath, J. A.; Montzka, D.; Richter, D.; Ullmann, K.; Walega, J.; Weibring, P.; Weinheimer, A.; Staebler, R. M.; Liao, J.; Huey, L. G.; Kleffmann, J. Nitrous Acid (HONO) during Polar Spring in Barrow, Alaska: A Net Source of OH Radicals? *Journal of Geophysical Research Atmospheres* **2011**, *116* (24), 1–12. https://doi.org/10.1029/2011JD016643.

(36) Spataro, F.; Ianniello, A.; Salvatori, R.; Nardino, M.; Esposito, G.; Montagnoli, M. Sources of Atmospheric Nitrous Acid (HONO) in the European High Arctic. *Rendiconti Lincei* **2017**, *28* (1), 25–33. https://doi.org/10.1007/s12210-016-0568-9.

(37) Acker, K.; Möller, D.; Wieprecht, W.; Meixner, F. X.; Bohn, B.; Gilge, S.; Plass-Dülmer, C.; Berresheim, H. Strong Daytime Production of OH from HNO2 at a Rural Mountain Site. *Geophys Res Lett* **2006**, *33* (2), 2–5. https://doi.org/10.1029/2005GL024643.

(38) Kleffmann, J.; Wiesen, P. Technical Note: Quantification of Interferences of Wet Chemical HONO LOPAP Measurements under Simulated Polar Conditions. *Atmos Chem Phys* **2008**, *8* (22), 6813–6822. https://doi.org/10.5194/acp-8-6813-2008.

(39) Ye, C.; Gao, H.; Zhang, N.; Zhou, X. Photolysis of Nitric Acid and Nitrate on Natural and Artificial Surfaces. *Environ Sci Technol* **2016**, *50* (7), 3530–3536. https://doi.org/10.1021/acs.est.5b05032.

(40) Bao, F.; Li, M.; Zhang, Y.; Chen, C.; Zhao, J. Photochemical Aging of Beijing Urban PM2.5: HONO Production. *Environ Sci Technol* **2018**, *52* (11), 6309–6316. https://doi.org/10.1021/acs.est.8b00538.

(41) Baergen, A. M.; Donaldson, D. J. Photochemical Renoxification of Nitric Acid on Real Urban Grime. *Environ Sci Technol* **2013**, *47* (2), 815–820. https://doi.org/10.1021/es3037862.

(42) Oswald, R.; Behrendt, T.; Ermel, M.; Wu, D.; Su, H.; Cheng, Y.; Breuninger, C.; Moravek, A.; Mougin, E.; Delon, C.; Loubet, B.; Pommerening-Röser, A.; Sörgel, M.; Pöschl, U.; Hoffmann, T.; Andreae, M. O.; Meixner, F. X.; Trebs, I. HONO Emissions from Soil Bacteria as a Major Source of Atmospheric Reactive Nitrogen. *Science (1979)* **2013**, *341* (6151), 1233–1235. https://doi.org/10.1126/science.1242266.

(43) Su, H.; Cheng, Y.; Oswald, R.; Behrendt, T.; Trebs, I.; Meixner, F. X.; Andreae, M. O.; Cheng, P.; Zhang, Y.; Pöschl, U. Soil Nitrite as a Source of Atmospheric HONO and OH Radicals. *Science (1979)* **2011**, *333* (6049), 1616–1618. https://doi.org/10.1126/science.1207687.

(44) George, C.; Strekowski, R. S.; Kleffmann, J.; Stemmler, K.; Ammann, M. Photoenhanced Uptake of Gaseous NO2 on Solid Organic Compounds: A Photochemical Source of HONO? In *Faraday Discussions*; 2005; Vol. 130, pp 195–210. https://doi.org/10.1039/b417888m.